Modeling Communication Reliability in LoRa Networks with Device-level Accuracy

Verónica Toro-Betancur*, Gopika Premsankar*, Mariusz Slabicki§†, and Mario Di Francesco*

{veronica.torobetancur, gopika.premsankar, mario.di.francesco}@aalto.fi, mariusz.slabicki@nokia.com

*Department of Computer Science
Aalto University

§Nokia Solutions and Networks
Wroclaw, Poland

†Institute of Theoretical and Applied Informatics
Polish Academy of Sciences

Abstract—**Long Range (LoRa) is a low-power wireless communication technology for long-range connectivity, extensively used in the Internet of Things. Several works in the literature have analytically characterized the performance of LoRa networks, with particular focus on scalability and reliability. However, most of the related models are limited, as they cannot account for factors that occur in practice, or make strong assumptions on how devices are deployed in the network. This article proposes an analytical model that describes the delivery ratio in a LoRa network with device-level granularity. Specifically, it considers the impact of several key factors that affect real deployments, including multiple gateways and channel variation. Therefore, the proposed model can effectively evaluate the delivery ratio in realistic network topologies, without any restrictions on device deployment or configuration. It also accurately characterizes the delivery ratio of each device in a network, as demonstrated by extensive simulations in a wide variety of conditions, including diverse networks in terms of node deployment and link-level parameter settings. The proposed model provides a level of detail that is not available in the state of the art, and it matches the simulation results within an error of a few percentage points.**

Keywords—*LoRa, analytical model, communication reliability*

I. INTRODUCTION

Long Range (LoRa) [1] is a popular wireless connectivity standard targeted for resource-constrained devices. In particular, LoRa provides long-range connectivity with a very low power consumption, which is especially suitable for applications in the Internet of Things (IoT). In this context, the number of LoRa-based networks is rapidly growing due to the relatively low cost of network setup [2] and the open-source nature of its networking standards [3]. As a result, LoRa is being extensively used in urban applications, smart metering, and precision agriculture [1, 2].

For these applications, LoRa devices periodically collect and then send data to one or more gateways for further processing or storage [2, 4]. In urban scenarios, devices are typically located inside buildings and can reach a density of 20,000 devices/km² or even more [5, 6]. The traffic of individual devices is sporadic and the size of messages is generally small. However, the challenging nature of the wireless channel in urban scenarios, together with the huge number of devices and the low data rate, make reliable communication particularly difficult [7]. This is especially true for application scenarios that cannot simply rely on sufficiently-high *average* reliability across the network, but also on a *minimum* reliability for individual devices. A representative use case is that of smart parking: remote sensors report the occupancy of parking spots to inform drivers about available spaces and also for billing purposes [8]. In fact, certain sensors might be in challenging

locations (i.e., at the corner of an underground parking facility), therefore, a large number of sent messages might be lost. Consequently, the parking spot could be considered occupied, while it is actually available. This reduces the profit of the parking control company, and it is also an inconvenience to drivers.

LoRa relies on different parameters at the physical layer that can be tailored for specific application requirements [9, 10], based on the actual network deployment [11]. The spreading factor (SF) and the transmission power (TP) are particularly important, as they affect the communication range of a device and the chance of message collisions [7, 11]. The spatial layout of the network determines an appropriate choice of SFs and TPs for the devices [10]. Specifically, the distance between devices and gateways impact on the available options which, in turn, affect the performance – particularly, the reliability – of the whole network.

Several works in the literature have characterized the performance of LoRa networks – with particular focus on scalability and reliability – by real experiments [12, 13], simulation [7, 14, 15], or analytical modeling [9, 16]. The latter approach is particularly useful, as it enables optimal parameter selection [10, 14] and flexible evaluation of different network scenarios, which would otherwise very time-consuming to simulate or even deploy [17]. To be valuable, however, an analytical model must be both *explanatory* and *accurate*, so as to capture the complexities of real-world LoRa deployments.

The state of the art (Section IV) has modeled LoRa networks by using stochastic geometry [9, 16, 18–20] or by extending well-known models for contention-based channel access [14, 21, 22]. However, these models consider simple network layouts with only one gateway [9, 16, 18, 19], or make strict assumptions about the spatial distribution of nodes [20]. Moreover, analytical models typically derive the overall (i.e., *aggregate*) delivery ratio in a network [21] or for a particular spreading factor [22]. However, simulation-based studies of LoRa networks have shown that a high delivery ratio for a certain SF does not imply that all devices using that SF experience the same [10]. In this respect, this article proposes an analytical model to obtain the delivery ratio for *each* device in a LoRa network.

The main contributions of this work are as follows. First, it **considers the impact of several key factors that affect real deployments**, including quasi-orthogonal transmissions under the capture effect, duty cycling, multiple gateways, and channel variation due to fading (Section II). Therefore, the proposed model can effectively evaluate the delivery ratio in realistic network topologies, without any restrictions on how devices are deployed or on how transmission parameters (i.e., SFs and

TPs) are assigned. Second, it **accurately characterizes the delivery ratio of each device in a network**, as demonstrated by extensive simulations in a wide variety of conditions, including diverse networks in terms of node deployment and link-level parameter settings (Section III). In particular, the proposed model provides a level of detail that is not available in the state of the art, and it matches the simulation results within an error of a few percentage points.

II. ANALYTICAL MODEL

This section presents a novel analytical model to evaluate the delivery ratio per node in a LoRa network. The considered scenario includes one or more gateways ($k \in \mathcal{M}$) that provide network connectivity to LoRa nodes ($n \in \mathcal{N}$). The traffic consists of unconfirmed messages (i.e., without acknowledgments and retransmissions) sent from nodes to the gateways, which is typical of LoRa-based sensing applications [2]. The physical layer in LoRa allows to set different transmission parameters – the most relevant ones are the *spreading factor* (SF) and the *transmission power* (TP). Specifically, the SF is the ratio between symbol and chip rates in the chirp spread spectrum modulation technique adopted by LoRa [7], ranging from 7 to 12. As a consequence, SFs trade off transmission range for data rate: the higher the SF, the higher the coverage range and the lower the data rate. Moreover, simultaneous transmissions are quasi-orthogonal, in the sense that the receiver may still be able to decode them if the source nodes are using different SFs [9]. Each node in the network can use different SFs and TPs to reach a gateway. For simplicity, radio propagation is assumed[1] to follow a log-distance path loss model [23]. Accordingly, the receive power of node n at gateway k ($P_{n,k}^r$) is given by:

$$P_{n,k}^r = P_n^t - \overline{PL}(d_0) - 10\gamma \log\left(\frac{d_{n,k}}{d_0}\right) - X_\sigma, \quad (1)$$

where P_n^t is the transmission power (TP), $\overline{PL}(d_0)$ is the mean path loss for distance d_0, $d_{n,k}$ is the distance to the gateway k, γ is the path loss exponent, and $X_\sigma = \mathcal{N}(0,\sigma)$ is a random variable following a Gaussian distribution with zero mean and standard deviation of σ. Clearly, the maximum coverage range depends on the TP but also on the sensitivity of the gateway, which varies for each SF [7].

The traffic pattern is described by a Poisson distribution to model the discrete and random nature of message transmissions typical of low-power wide area networks [9, 24]. Accordingly, the probability for a node to transmit k packets in a time interval T is given by:

$$f(k) = \frac{(\lambda T)^k e^{-\lambda T}}{k!}, \quad (2)$$

where λ is the average *sending rate*. Therefore, the probability of no transmissions occurring at time interval T in a network with N nodes is:

$$\mathbb{P}(k=0) = \prod_{i=1}^{N} e^{-\lambda T} = e^{-\lambda T N}. \quad (3)$$

The delivery ratio of a node n is derived next for a simple scenario with a single gateway and no variation in the channel

---

[1]Other radio propagation models could be easily considered as well.

TABLE I: Summary of used notation.

Symbol	Description
$P_{n,k}^r$	Receive power of node n at gateway k
P_n^t	Transmission power of node n
d_0	Minimum distance to a certain gateway
$\overline{PL}(d_0)$	Mean path loss for distance d_0
γ	Path loss exponent
σ	Standard deviation
T_s	Time-on-air for SF s
N_s	Set of nodes using SF s
λ	Average transmissions per unit time
D_n	Delivery ratio of node n
L	Number of preamble symbols
p_s	Time-on-air of one preamble symbol
$\mathcal{I}_n$	Set of interferers of node n
$\mathcal{I}_{n,s}$	Set of interferers of node n using SF s
$\mathcal{I}_n^k$	Set of interferers of node n with respect to gateway k
δ_s	Portion of ON-time due to duty cycle at SF s
$G(\mathcal{I}_n)$	Offered load by interfering nodes in $\mathcal{I}_n$
R_n^k	Set of nodes in the intersection of k vulnerability areas of n
$\mathcal{N}(\mu,\sigma)$	Normal distribution with mean μ and standard deviation σ
$E_{R_n^k}$	No transmission by the nodes in R_n^k
$E'_{R_n^k}$	Transmission by any of the nodes in R_n^k
C_j	Collision of the test node and an interferer j
$\mathbb{P}_o$	Probability of outage
$\mathbb{P}_c$	Probability of collision

(i.e., $\sigma = 0$), without considering the capture effect and duty cycling, and assuming perfect orthogonality between SFs. In doing so, the following terminology is used: *test node* denotes the device whose delivery ratio is being evaluated, whereas *interfering node (interferer)* indicates a different node that can interfere with the test node in case of a simultaneous transmission. According to the previously-described assumptions, a packet sent by test node n is not received by a gateway if at least one interfering node simultaneously transmits with the same SF s. Note that the time-on-air of packets depends not only on their length but also on the SF [25]. Therefore, transmissions overlap during the interval $T_s \leq t \leq T_s + \epsilon$ for the case of node n starting at time $t = T_s$ and an interferer j with SF s at time $t = T_s - \alpha$ where $T_s = \alpha + \epsilon$. Equivalently, node j does not interfere with node n as long as it does not start transmitting during $2T_s$. Such a time is referred to as the *interfering time frame*. Thus, the delivery ratio for node n with SF s can be derived as:

$$D_n = e^{-2\lambda T_s |N_s|}. \quad (4)$$

which corresponds to the delivery ratio for the unslotted ALOHA medium access scheme [7, 10]. Recall that the simple expression above has been obtained under quite restrictive assumptions. The following sections relax each of them by considering: the impact of imperfect SF orthogonality and the capture effect (Section II-A), duty cycling (Section II-B), multiple gateways (Section II-C), and shadowing (Section II-D). Table I summarizes the notation used in the rest of the article.

A. *Capture effect and quasi-orthogonality*

The *capture effect* allows a transmission to be successfully received even in presence of overlapping transmissions. This effect applies to all transmissions, for SFs that are the same or even different. In fact, transmissions in different SFs are actually *quasi-orthogonal*, in the sense that they are correctly

decoded only if the SIR of the target signal is above a certain threshold, as observed in [9, 26, 27]. The thresholds for the different pairs of SFs are defined by the SIR matrix [9, 26]:

$$\text{SIR} = \begin{pmatrix} 1 & -8 & -9 & -9 & -9 & -9 \\ -11 & 1 & -11 & -12 & -13 & -13 \\ -15 & -13 & 1 & -13 & -14 & -15 \\ -19 & -18 & -17 & 1 & -17 & -18 \\ -22 & -22 & -21 & -20 & 1 & -20 \\ -25 & -25 & -25 & -24 & -23 & 1 \end{pmatrix} \quad (5)$$

whose rows represent the SF of the test node and the columns the SF of the interferer, with SFs increasing with the row/column indices (i.e., from SF7 until SF12). The set $\mathcal{I}_n$ denotes the interferers for node n, and its elements are derived for the case of node n using SF s as:

$$\mathcal{I}_n = \left\{ j \mid P_n^r - P_j^r < \text{SIR}_{s,s'}, \forall j, s' \right\}, \quad (6)$$

where $\text{SIR}_{s,s'}$ is the SIR threshold for the test node n using SF s and the interfering node j using SF s'. Let us consider an illustrative example wherein the test node n uses SF7 and the potential interferer j uses SF12: if the difference of their receive power at the gateway is below -9 dB [Eq. (5)], then j actually interferes with n (i.e., j is an interferer).

The SIR thresholds establish that the set of interferers depends not only on the SFs, but also on the location of the nodes in the network. The latter aspect is characterized through the concept of *vulnerability areas* as defined in [22]. Specifically, a vulnerability area is the region containing all the interfering nodes for a given test node, derived according to a SIR threshold [22, 28]. Clearly, the higher the threshold, the larger the area and the number of nodes possibly contained therein. Moreover, given a test node, there are different vulnerability areas depending on the SF (i.e., one for each of them).

Modeling the capture effect requires considering that different SFs result in different transmission times, even for packets with the same packet length [25]. Therefore, the probability that no interferers transmit during $2T_s$ time for a test node n using SF s (as derived at the beginning of the section) is no longer sufficient in this case. In fact, the time-on-air of both the test node (T_s) and the interferer node ($T_{s'}$) have to be taken into account. Moreover, it has been experimentally determined that LoRa packets can still be successfully decoded when the last five preamble symbols are received correctly, even if the rest of the preamble is subject to interference [7]. As a consequence, an interferer transmitting during the first part of the preamble sent by the test node does not result in packet loss. Accordingly, the interference time frame becomes:

$$T_s' = T_s + T_{s'} - (L - 5)p_s, \quad (7)$$

where L is the total number of preamble symbols and p_s is the time-on-air of one preamble symbol sent by the test node with SF s, as illustrated in Figure 1. Therefore, the delivery ratio of node n under the capture effect becomes:

$$D_n = \prod_{s'=7}^{12} e^{-\lambda T_{s'}' \mathcal{I}_{n,s'}} = \exp\left(-\lambda \sum_{s'=7}^{12} T_{s'}' \mathcal{I}_{n,s'} \right) \quad (8)$$

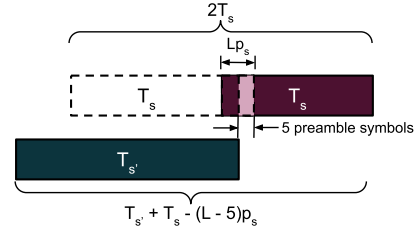where $\mathcal{I}_{n,s'}$ is the set of interferers of node n that use SF s'.

Fig. 1: LoRa packets from test node and interferer with details of preamble and interference time frame.

B. Duty cycle

As LoRa networks operate in unlicensed bands, nodes must follow country-specific restrictions, which include a maximum duty cycle δ to limit transmissions [3, 9, 25]. For instance, a duty cycle of at most 1% is enforced in Europe for transmissions[2] in the 868 MHz band. The duty cycle consists of an active period, during which a packet is transmitted, and of an inactive period, wherein no packets are transmitted. The duration of the active period depends on the time-on-air T_s for a packet sent with SF s and its probability can be derived based on the Poisson distribution of traffic. In particular, let δ_s be the probability of a node being in an active period at a given time. Then, the packet sending rate becomes $\lambda \delta_s$, following the thinning property of the Poisson process [9, 29]. As a consequence, a node transmits during a fraction of time λT_s, after which it remains inactive for a fraction of time equal to $100(1 - \delta)\lambda T_s$. Accordingly, δ_s is given by:

$$\delta_s = 1 - 100(1 - \delta)\lambda T_s \qquad \forall s \in \{7, 8, ..., 12\}. \quad (9)$$

Note that the resulting sending rate is $\lambda \delta_s$, thus, the delivery ratio in presence of a duty cycle is:

$$D_n = \exp\left(-\lambda \sum_{s'=7}^{12} T_{s'}' \mathcal{I}_{n,s'} \delta_{s'} \right) \quad (10)$$

To simplify notation, the sum over s' is denoted as $G(\mathcal{I}_n)$, i.e., $G(\mathcal{I}_n) = \sum_{s'=7}^{12} T_{s'}' N_{s'} \delta_{s'}$. Then, the duty cycle becomes:

$$D_n = e^{-\lambda G(\mathcal{I}_n)} \quad (11)$$

C. Multiple gateways

Nodes in a LoRa network are not associated with a single gateway, thus, their transmissions can be received by any gateway in range. The gateways forward all received messages to a network server, which discards possible duplicates. This feature is very important for scalability in large networks [10], therefore, it must be accounted for in deriving the delivery ratio. To this end, the sets of interferers are considered both per node and per gateway.

As an illustration, Figure 2 shows a network with two gateways (triangles), a test node n (star), its vulnerability areas[3] for each gateway (dashed circles), interfering nodes

---

[2] Accordingly, a node must be inactive for a duration of at least 99 times the time-on-air of the last packet sent, after its transmission.

[3] For clarity, the example depicts vulnerability areas as circles by assuming that all nodes use the same TP and SF.
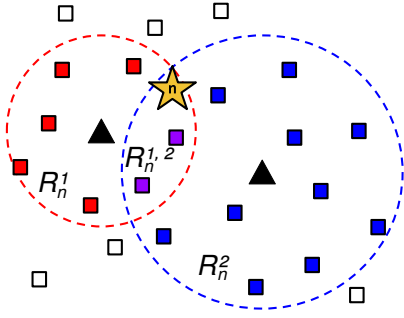
Fig. 2: Sample network with two gateways, a test node n, its vulnerability areas (dashed circles), interferers (filled squares) and other nodes (empty squares).

(filled squares), and other nodes (empty squares). Let $\mathcal{I}_n^1$ and $\mathcal{I}_n^2$ be the sets of the interfering nodes within the corresponding vulnerability areas. Without loss of generality, $\mathcal{I}_n^1 \cap \mathcal{I}_n^2 \neq \varnothing$. The sets of interfering nodes located in the areas delimited by the intersecting circles are referred to as *regions*. For instance, Figure 2 defines three regions: R_n^1 and R_n^2 with the nodes that can only reach a single gateway; and $R_n^{1,2}$ with nodes that can reach both gateways. Note that, the intersection between any pair of regions is empty by definition, since $R_n^1 = \mathcal{I}_n^1 \setminus \mathcal{I}_n^2$, $R_n^2 = \mathcal{I}_n^2 \setminus \mathcal{I}_n^1$ and $R_n^{1,2} = \mathcal{I}_n^1 \cap \mathcal{I}_n^2$.

The delivery ratio per node in a scenario with multiple gateways can be derived by considering all possible factors preventing the packets sent by test node n to be received by *any* gateway. In particular, a collision occurs in the case of Figure 2 when: *at least one* node in $R_n^{1,2}$ transmits during the interference time frame of n; **or** *at least one* node in R_n^1 **and** *at least one* node in R_n^2 transmit during the interference time frame of the test node n.

The first condition can be equivalently expressed as the negation of the probability that none of the nodes in $R_n^{1,2}$ transmit during the corresponding interference time frame (see Section II-A). Let $E_{R_n^{1,2}}$ denote the event of no transmitting nodes in $R_n^{1,2}$ and $E'_{R_n^{1,2}}$ its complement (i.e., at least one node transmitting in $R_n^{1,2}$) – the associated probabilities are indicated by $\mathbb{P}(E_{R_n^{1,2}})$ and $\mathbb{P}(E'_{R_n^{1,2}})$. Then, it is:

$$\mathbb{P}(E'_{R_n^{1,2}}) = 1 - \mathbb{P}(E_{R_n^{1,2}}) = 1 - e^{-\lambda G(R_n^{1,2})}.$$

The second condition is the conjunction between the events of at least one transmitting node in regions R_n^1 and R_n^2:

$$\mathbb{P}\left(E'_{R_n^1} \cap E'_{R_n^2}\right) = (1 - \mathbb{P}(E_{R_n^1}))(1 - \mathbb{P}(E_{R_n^2}))$$
$$= \left(1 - e^{-\lambda G(R_n^1)}\right)\left(1 - e^{-\lambda G(R_n^2)}\right)$$

where the corresponding events and probabilities are defined similarly to the previous case. The delivery ratio of a node n can be finally expressed as:

$$D_n = 1 - \mathbb{P}\left(E'_{R_n^{1,2}} \cup \left(E'_{R_n^1} \cap E'_{R_n^2}\right)\right)$$
$$= e^{-\lambda G(R_n^{1,2})} \cdot \left[e^{-\lambda G(R_n^1)} + e^{-\lambda G(R_n^2)} - e^{-\lambda G(R_n^1 \cup R_n^2)}\right]$$

whose derivation relies on the De Morgan's laws and the general disjunction rule for two events.

The general case of a network with m gateways requires considering the regions corresponding to all possible intersections of the vulnerability areas, namely, $\sum_{i=1}^m \binom{m}{i}$ regions. For instance, a network with three gateways has seven regions: three regions with nodes that can only reach one gateway; three regions with nodes that can reach exactly two gateways; and one region with nodes that can reach all the gateways.

After determining such regions, it remains to derive under which conditions a packet sent by the test node is not successfully received by any gateway. This involves considering all possible gateways reachable by the test node, particularly, the sets of regions described above that cover all the reachable gateways. This corresponds to finding the *set covers*, a well-known NP-complete problem which has been extensively addressed in the literature [30–32]. In this context, the set cover problem is defined as enumerating all sets of regions that cover all the gateways, such as, if at least one of the interferers from each of such regions transmit simultaneously as the test node, then the packet sent by the test node will not be received by any of the gateways. Nodes in typical LoRa deployments can reach at most four gateways in practice [4]. Thus, the possible set covers have small cardinality and can be quickly found. For instance, $\{R_n^{1,2}\}$ and $\{R_n^1, R_n^2\}$ are the set covers for the scenario in Figure 2, since the regions in each set cover account for all the gateways (1 and 2).

Let $\mathcal{S}$ be the set of set covers of all possible regions in intersecting vulnerability areas. The delivery ratio in the general case of m gateways is then given by:

$$D_n = 1 - \mathbb{P}\left(\bigcup_{i=1}^{|\mathcal{S}|}\left(\bigcap_{R_n^k \in \mathcal{S}_i} E'_{R_n^k}\right)\right)$$
$$= \prod_{i=1}^{|\mathcal{S}|}\left(1 - \left(\prod_{R_n^k \in \mathcal{S}_i}\left(1 - e^{-\lambda G\left(R_n^k\right)}\right)\right)\right) \quad (12)$$

Again, the derivation relies on the De Morgan's laws and on the fact that all regions are disjoint, to express the probability of the conjunction between multiple terms as a product.

Finally, the path loss model in Eq. (1) is calculated for all nodes with respect to all gateways to determine the sets of interferers per gateway $\mathcal{I}_n^k, \forall k \in \{1, 2, \ldots, m\}$ by using Eq. (6). Note that the delivery ratio in Eq. (12) becomes the one in Eq. (11) when $m = 1$, since $R_n^k = \varnothing \ \forall k \neq 1$ and R_n^1 becomes $\mathcal{I}_n, \forall n \in \mathcal{N}$.

D. Channel variation

So far, no channel variation was considered, i.e., $\sigma = 0$ was assumed. Such an assumption is relaxed next by introducing shadow fading (i.e., $\sigma \neq 0$). For clarity, a single gateway scenario is addressed first, and then extended to multiple gateways.

Single gateway. The path loss model in Eq. (1) for test node n and interferer j can be rewritten as:

$$P_i^r = a_i + X_i, \quad (13)$$

where $i \in \{n, j\}$, $a_i = P_i^t - \overline{PL}(d_0) - 10\gamma \log(d_i/d_0)$ and $X_i = \mathcal{N}(0, \sigma \neq 0)$. The following holds for each interferer j:

$$P_n^r - P_j^r < \text{SIR}_{s,s'} \quad (14)$$

Following Eq. (13), the previous expression can be written as:

$$X_1 - X_2 < b - (a_1 - a_2)$$

for the case of $n = 1, j = 2$ and $\text{SIR}_{s,s'} = b$. The difference between two zero-mean normal distributions with standard deviation σ is another zero-mean normal distribution with standard deviation 2σ [33]. Let $X_3 = X_1 - X_2$ denote such a distribution. Then, its probability density function is:

$$f(X_3) = \frac{1}{2\sigma\sqrt{2\pi}} e^{-\frac{X_3^2}{8\sigma^2}}. \tag{15}$$

Finally, the probability that X_3 is smaller that $b - (a_1 - a_2)$ is:

$$\mathbb{P}(X_3 < b-(a_1-a_2)) = \frac{1}{2}\left[\text{erf}\left(\frac{b-(a_1-a_2)}{2\sigma\sqrt{2}}\right) + 1\right] \tag{16}$$

where erf is the error function [33].

In scenarios without shadow fading, any simultaneous transmissions of a test node and an interferer collide at the gateway, preventing successful packet reception. With shadow fading, instead, collisions occur with a probability $\mathbb{P}_c$ that takes channel variation into account. In addition, the receive power of a signal may be below the sensitivity of the gateway due to shadow fading. This is characterized as an outage probability $\mathbb{P}_o$. The delivery ratio of node n is then defined as:

$$D_n = (1 - \mathbb{P}_c)(1 - \mathbb{P}_o)$$

The derivation of the two probabilities is detailed next.

Recall that $\mathbb{P}_c$ is the probability that at least one interfering node transmits during the interference time frame of node n ($E'_{\mathcal{I}_n}$), with enough power to cause interference. Therefore:

$$\mathbb{P}_c = \mathbb{P}\left(\bigcup_{j \in \mathcal{I}_n} (E'_{\{j\}} \cap C_j)\right) \tag{17}$$

where: $\mathbb{P}(E'_{\{j\}}) = 1 - e^{-\lambda G(\{j\})}$, with $j \in \mathcal{I}_n$, as in Section II-C; and $\mathbb{P}(C_j)$ is the probability of node j interfering with node n, according to Eq. (16):

$$\mathbb{P}(C_j) = \frac{1}{2}\left[\text{erf}\left(\frac{b-(a_n-a_j)}{2\sigma\sqrt{2}}\right) + 1\right]$$

with $j \in \mathcal{I}_n$. Note that Eq. (17) can be rewritten as:

$$\mathbb{P}_c = 1 - \prod_{j \in \mathcal{I}_n}\left(1 - \mathbb{P}(E'_{\{j\}})\mathbb{P}(C_j)\right) \tag{18}$$

in terms of only conjunctions, since the probabilities of transmission and interference of each node are independent. The derivation of $\mathcal{I}_n$ still relies on the vulnerability areas (as defined in Section II-A), which are extended through σ to account for all interfering nodes in presence of channel variation. Specifically, a factor of 2σ is added to the thresholds in the SIR matrix [following Eq. (15)].

Finally, the outage probability for test node n with SF s is:

$$\mathbb{P}_o = \frac{1}{2}\left[\text{erf}\left(\frac{P_n^t - P_{\text{sens},s} - \overline{PL}(d_0) - 10\gamma\log\left(\frac{d_n}{d_0}\right)}{\sigma\sqrt{2}}\right) + 1\right]$$

where $P_{\text{sens},s}$ is the receiver sensitivity for SF s.

Multiple gateways. For a scenario with multiple gateways, the delivery ratio in Eq. (12) needs to include the probability of interference $\mathbb{P}(C_j)$ in addition to the probability of outage $\mathbb{P}_o$. Moreover, the probability of interference at each gateway varies across interferers.

Note that a node can belong to multiple regions formed by the intersections of vulnerability areas (Section II-A) in this case. Moreover, the interference probabilities with respect to different gateways are independent, as the paths from the nodes to each gateway are independent under shadow fading. Similarly, the interference probability associated with two gateways (or any other set of gateways) is also independent. As an illustration, recall Figure 2 and let j be an interferer that reaches two gateways, i.e., j is located at the intersection of the two vulnerability areas. When node j transmits, there is a probability of interference with the first gateway ($\mathbb{P}(C_j^1)$), another independent probability for the second gateway ($\mathbb{P}(C_j^2)$), and yet another one (also independent) for the two gateways ($\mathbb{P}(C_j^1 \cap C_j^2)$). As a result, node j is included in three regions: namely, R_n^1, R_n^2 and $R_n^{1,2}$.

Accordingly, the probability of collision is given by:

$$\mathbb{P}_c = \prod_{i=1}^{|\mathcal{S}|}\left(1 - \left(\prod_{R_n^k \in \mathcal{S}_i}\left(1 - \prod_{j \in R_n^k}\left(1 - \mathbb{P}(E'_{\{j\}})\mathbb{P}(C_j^k)\right)\right)\right)\right) \tag{19}$$

which, different from Eq. (12), considers each interferer independently to account for its interference probability with respect to all possible (sub)sets of gateways.

In addition, the probability of outage is calculated as the probability that the receive power is below the sensitivity of all gateways in range ($\mathbb{P}_o^k, \forall k \in \mathcal{M}$). Finally, the delivery ratio for the general case is:

$$D_n = (1 - \mathbb{P}_c)\left(1 - \prod_{k \in \mathcal{M}} \mathbb{P}_o^k\right) \tag{20}$$

Note that, this equation also applies for a single gateway network, when $m = 1$, since $R_n^k = \varnothing \;\forall k \neq 1$, R_n^1 becomes $\mathcal{I}_n^1$ and $\mathbb{P}_o = \mathbb{P}_o^1, \forall n \in \mathcal{N}$.

III. EVALUATION

This section presents the results from evaluating the performance of the proposed model through extensive simulations. Specifically, the evaluation measures how accurately the delivery ratio derived by the model follows those obtained through simulations. To this end, simulations are performed using the open-source FLoRa simulator [15] with the settings in Table II. The path loss model uses the parameters defined in [7] based on measurements in an urban scenario.

The evaluation includes scenarios with different network layouts and different assignments of SFs and TPs, with either no channel variation ($\sigma = 0$) or shadow fading ($\sigma = 3.57$ dB [7]). In all scenarios, the network layouts are such that all nodes can reach at least one gateway. Each experiment runs for seven days of simulated time and twenty independent replications are carried out. The spread in the results is reported with 95% confidence intervals where meaningful.

TABLE II: Simulation parameters.

Parameter	Value
λ	0.001 s^{-1}
Duty cycle (δ)	0.01
Path loss	Eq. 1 with $\overline{PL}(d_0)$ = 127.41 dBm, $d_0 = 40\,\text{m}$, $n = 2.08$, $\sigma = \{0,\ 3.57\}$
Packet length	20 bytes
Preamble length	8 bytes
Frequency	868 MHz
Bandwidth	125 kHz
Coding rate	4/8
SFs	$\{7,\ 8,\ 9,\ 10,\ 11,\ 12\}$
TPs	$\{2,\ 5,\ 8,\ 11,\ 14\}$ dBm

The delivery ratio is measured as the number of packets that are successfully received by at least one gateway divided by the number of packets sent, expressed as a percentage. The accuracy of the proposed model with respect to the simulation results is measured using the mean absolute error (MAE):

$$\text{MAE} = \frac{1}{|\mathcal{N}|} \sum_{i \in \mathcal{N}} |y_i - \hat{y}_i|, \qquad (21)$$

where $\mathcal{N}$ is the set of all nodes in the network and y_i and $\hat{y}_i$ are the delivery ratio of node i as predicted by the model and obtained through simulations, respectively.

The following first characterizes the model accuracy in different scenarios, then compares it against the state of the art. Next, the impact of the different model elements on the derived delivery ratio is considered. Finally, the accuracy of the proposed model is evaluated in non-uniform networks.

A. Accuracy under different settings

The accuracy of the proposed model is evaluated under three scenarios by varying the number of nodes, the number of gateways, and the assignment of SFs as well as TPs. Figure 3 shows the results from each scenario as box plots.

In the first scenario (Figure 3a), the accuracy of the model is evaluated in networks comprising 500, 1,000, 1,500 and 2,000 nodes uniformly distributed around a gateway within a radius of 544 m (the maximum coverage range in this scenario). All nodes use the highest TP of 14 dBm. The nodes are assigned the smallest SF that allows them to reach the gateway [16, 21]. Figure 3a presents the MAE between the model and the simulation for each iteration. In all cases with $\sigma = 3.57$, the model derives the delivery ratio for each node with an average error of less than 6% and a low spread across the iterations. For scenarios without shadow fading, the model consistently achieves an MAE of less than 1.5%. Nevertheless, the MAE increases slightly with the number of nodes, mostly in cases with shadowing. This is caused by the nodes using SF12. In particular, the SF assignment policy allocates SF12 to the nodes in the outer ring of the network, thus, these have the largest sets of interferers. For this reason, the model tends to slightly underestimate their delivery ratio.

In the second scenario (Figure 3b), the number of nodes is set to 1,000 and the number of gateways is varied from 2 to 4. Figure 4 illustrates the locations of the gateways in the evaluated networks, wherein the rectangles are the deployed

areas and the black triangles are the gateways. Such locations were chosen to represent networks where gateways are not too close to each other and still some coverage areas overlap. Nodes are placed uniformly in the deployment area. Also in this scenario, the nodes are assigned the highest TP and the minimum SF that allows them to reach at least one gateway. The distribution of MAEs for each iteration is shown in Figure 3b. The model characterizes well the impact of multiple gateways and overlapping regions, with a low MAE between 0.35% and 0.75% in scenarios with $\sigma = 0$ and from 1.0% to 1.7% with shadow fading. The MAE in all the considered networks with multiple gateways is smaller than that for a single gateway (Figure 3a, for 1,000 nodes). This is because there are more regions to consider with more gateways (recall Figure 2) and fewer nodes per region. Hence, the overall MAE is lower when smaller sets of nodes are considered in the regions. It is also important to note that deriving the delivery ratio per node using the presented model is significantly faster than using simulations. For instance, on a machine with an Intel Core i5-7300U CPU and 16 GB of RAM, the model obtains the delivery ratios for a network with 2,000 nodes and 4 gateways in 10 minutes, as opposed to the 7 hours needed to carry out simulations.

The last scenario (Figure 3c) considers three different SF and TP assignment policies in networks comprising one gateway and 1,000 nodes uniformly distributed around the gateway. The policies chosen are as follows. The first policy randomly assigns SFs according to a uniform distribution and sets the TPs of all nodes to the highest value of 14 dBm. In the second policy, the nodes use the lowest SF that allows them to reach the gateway. The TP for each node is randomly chosen between the two highest available values (11 dBm and 14 dBm). Such a policy allows the nodes to reach the gateway while having a heterogeneous distribution of TPs. Finally, the third policy uses the OPT-DELTA and OPT-TP mixed-integer linear programming models presented in [10], respectively, to assign SFs and TPs. The solutions to the optimization models are obtained through IBM ILOG CPLEX (version 12.7.1). This policy is chosen to represent networks wherein the SFs and TPs of the nodes are not purely assigned based on their distance to the gateway[4]. The radius of the deployed area is 100 m for networks configured with the first policy, and 365 m for the others. A smaller radius is chosen for the first policy to evaluate scenarios where the SFs are uniformly assigned over the whole area, and all nodes can reach the gateway with any SF. In contrast, the second and third policies have to assign SF12 to the nodes farthest away from the gateway so that they are in communication range. The MAEs obtained for each policy are depicted in Figure 3c. It can be seen that, the model consistently achieves a MAE of less than 2.1%. Nevertheless, the delivery ratios in networks with a random assignment of SFs are obtained with a slightly higher accuracy. This is again due to the outer ring of nodes with SF12 that is present in networks configured with OPT-DELTA and minimum SF.

All the presented results demonstrate that the proposed analytical model derives the delivery ratio with high accuracy, independent from the number of nodes or gateways in the network and the SF/TP assignment policies.

---

[4]Specifically, OPT-DELTA assigns SFs to balance collisions in each SF for all gateways and OPT-TP assigns TPs to minimize energy consumption.
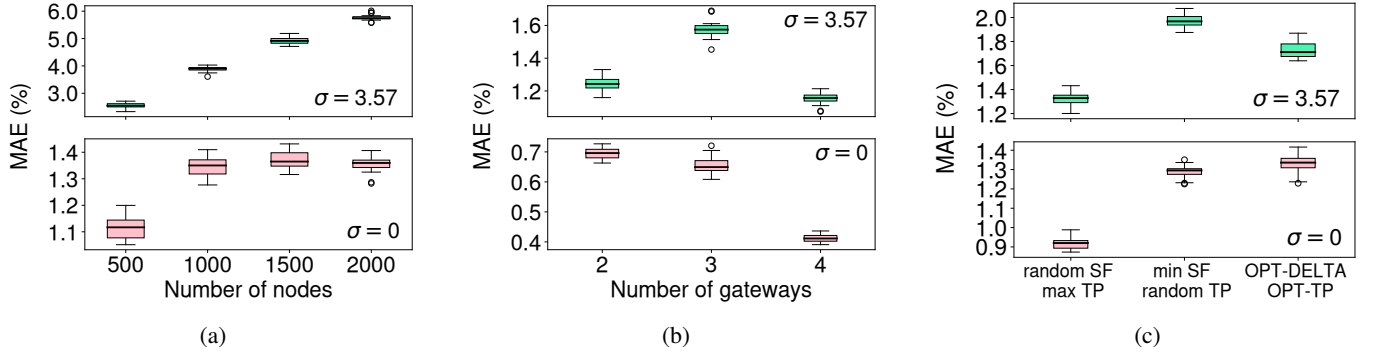
Fig. 3: MAE between the model and simulations for different (a) number of nodes, (b) number of gateways, and (c) SF and TP assignment policies.
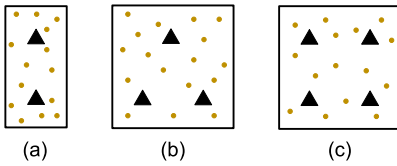

Fig. 4: Position of gateways in evaluated networks with (a) two, (b) three and (c) four gateways.

B. Comparison with state of the art

The following compares the proposed model against that in Croce et al. [22], which derives the average delivery ratio *per SF* in LoRa networks. The work in [22] was chosen as it does not impose any restrictions on the SF assignment policy or radio propagation model.

The evaluation is carried out in a network with one gateway and 1,200 nodes uniformly distributed within a radius of 300 m around the gateway. The nodes are randomly assigned SFs from those available (Table II). No channel variation or duty cycle are considered in this scenario, since they are not supported by [22]. Moreover, as required in [22], the SIR thresholds for inter-SF interference are constant for a node using a particular SF and independent of the SF used by the interfering node. Specifically, the inter-SF SIR thresholds are set to -9 dB, -12 dB, -13 dB, -18 dB, -21 dB and -25 dB for SFs 7, 8, 9, 10, 11 and 12, respectively. The co-SF SIR thresholds are set to 1 dB. The results refer to a single network instance, as the related 95% confidence interval for different layouts with 1,500 nodes and $\sigma = 0$ is very low (Figure 3a).

The average delivery ratio obtained by nodes using each SF is compared with that derived from [22] (Figure 5a). The delivery ratio in each SF is very similar in both approaches. However, the per-device delivery ratio obtained from our model reveals that the average delivery ratio per SF does not accurately characterize the values of individual nodes. In fact, the histograms (obtained from simulations) for delivery ratio of individual nodes using SF11 and SF12 (Figure 5b) show that their distribution does not correspond to the overall average delivery ratio per SF. In particular, some of the nodes can reach a delivery ratio of 100%, even though the average value obtained

by the model in [22] is 70.45% and 52.23% for SF11 and SF12, respectively (vertical dashed lines). More importantly, some nodes reach lower delivery ratios. In particular, for SF12, 43.68% of the nodes achieve a delivery ratio below 32.94%, which is around 20% less than that reported by the average delivery ratio. A per-device model, on the other hand, is able to derive such behavior of the individual nodes (Figure 5c) with a high accuracy when compared to the simulations[5]. Thus, the proposed model provides important additional insights that are not available when derived per SF.

C. Impact of different elements in the model

The impact of each model element on the derived delivery ratio is evaluated next. Specifically, the following elements are added one-by-one to the model – quasi-orthogonality as well as capture effect, duty cycle constraints, and shadowing – to evaluate how the obtained delivery ratio varies. In particular, the following model variations are considered: (a) ALOHA, without quasi-orthogonal SFs, capture effect, shadowing or duty cycle (i.e., nodes can transmit at any time and $\delta = 1$); (b) quasi-orthogonal SFs[6], no shadowing and no duty cycle ($\sigma = 0$, $\delta = 1$); (c) quasi-orthogonal SFs, shadowing and no duty cycle ($\sigma = 3.57$, $\delta = 1$); and (d) quasi-orthogonal SFs, shadowing and a duty cycle of 1% ($\sigma = 3.57$, $\delta = 0.01$).

The elements are evaluated in a network with one gateway and 1,000 nodes deployed uniformly around it within a radius of 100 m. The SFs are randomly assigned according to a uniform distribution and the TP is 14 dBm for all the nodes. Figure 6a shows the cumulative distribution function (CDF) of the results obtained by simulation (including all the effects) and model variations. Table III reports the average MAE and related 95% confidence intervals.

The results clearly show that all the elements of the model significantly affect how the deliver ratio is close to that in the simulation. However, shadowing and imperfect orthogonality have the highest impact. In particular, the ALOHA model achieves an MAE 7.3 times higher the complete model (with all the considered factors). Moreover, the model variant with

---

[5]The CDF reports the results from one simulation run as the mean MAE and 95% confidence interval over twenty iterations is 2.07 ± 0.014.

[6]Note that quasi-orthogonal SFs implies that both inter-SF and co-SF interference with the capture effect according to the SIR matrix are included.
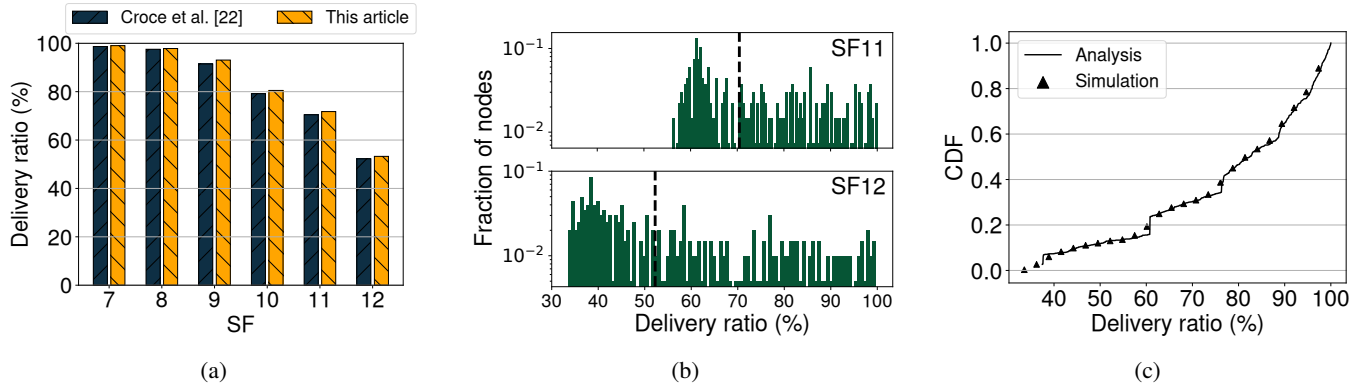
Fig. 5: (a) Comparison of the delivery ratio per SF achieved by the model and the one in [22], (b) histograms for delivery ratio of nodes with SF11 (top) and SF12 (bottom) and (c) CDF of the model with simulation results.

TABLE III: Average MAE for different model variations.

Model	ALOHA	$\sigma = 0,$ $\delta = 1$	$\sigma = 3.57,$ $\delta = 1$	$\sigma = 3.57,$ $\delta = 0.01$
MAE (%)	9.66 ± 0.16	3.59 ± 0.11	1.58 ± 0.03	1.32 ± 0.02

quasi-orthogonal SFs and no channel variation ($\sigma = 0$, $\delta = 1$) produces an MAE that is 2.7 times higher than the complete model. This shows that an accurate model for LoRa networks must include all the elements discussed thus far. In fact, evaluating the scalability of networks without considering these factors [10, 22] may produce unreliable results.

D. Node and link diversity

Next, two scenarios are considered to account for different types of diversity: nodes not uniformly distributed throughout the deployment area or around one gateway; and SFs assigned on a per-link basis according to the observed conditions.

Figure 6b illustrates node deployment in the first scenario: nodes are distributed in clusters and assigned different SFs (according to the colors indicated in the figure), to represent three buildings where LoRa sensors are deployed for metering purposes. Only one gateway (triangle in the figure) collects data from the nodes. All nodes transmit using the highest TP of 14 dBm. Figure 6c depicts the CDF of the delivery ratio obtained through simulation and derived from the model. Clearly, the model derives the delivery ratio of all the nodes with a high accuracy. Specifically, the MAE is 0.922% and the maximum difference in the observed delivery ratio is 5.708%.

Next, a non-uniform assignment of SFs and TPs is considered. Specifically, the network relies on Adaptive Data Rate (ADR) [11, 15], a standard algorithm, to assign such parameters in LoRa networks. The network comprises one gateway and 1,000 nodes uniformly distributed around it within a radius of 300 m. Initially, the nodes are configured with the lowest SF that allow them to reach the gateway. Next, simulations are first run with ADR enabled, namely, the nodes are assigned new SFs and TPs by the ADR algorithm. Figure 7a shows the resulting configuration. A separate simulation is then run by using the obtained SFs and TPs to compare the delivery ratio

with that derived by the model (Figure 7b). The figure shows that the distribution of the delivery ratio is very similar with both the approaches. Again, the model derives the delivery ratios with a high accuracy in networks where SFs are not uniformly distributed, with several nodes obtaining a low delivery ratio as found in [15]. Finally, Figure 7c shows the MAE calculated between the proposed model and simulations for the two scenarios described above. The low variance in the data shows that the proposed model is able to characterize the delivery ratio obtained through simulations with a high accuracy.

IV. RELATED WORK

Several works have applied stochastic geometry to model the delivery ratio in LoRa networks [9, 16, 18, 20]. Georgiou and Raza [16] obtain closed-form equations for the delivery ratio in networks with a single gateway. However, they consider only the strongest interferer within the same spreading factor in their analysis. Duda and Heusse [19] extend this model (from [16]) for an inhomogeneous distribution of nodes around the gateway. Specifically, the density of nodes decreases with the inverse square distance from the gateway, however with the same considerations of the strongest interferer. Next, Mahmood et al. [9] evaluate the delivery ratio in LoRa networks with a single gateway, by taking into account quasi-orthogonal spreading factors, the capture effect and duty cycle constraints. Similarly, Waret et al. [18] evaluate the delivery ratio in networks with a single gateway; however, their formulation does not include duty cycle constraints. Finally, Beltramelli et al. [20] apply stochastic geometry to model the delivery ratio in LoRa networks with multiple gateways. The formulation makes assumptions about the spatial distributions of gateways and nodes (such as a minimum distance between gateways) to obtain a tight lower bound on the estimated delivery ratio. However, all the models based on stochastic geometry obtain closed form equations based on the assumption that nodes transmit with the same power and are assigned spreading factors based on their distance to the gateway. This is not necessarily true in real LoRa networks, especially when ADR is used to assign spreading factors and transmission powers to the nodes [34]. Thus, such models cannot be used to evaluate more general spreading factor allocations, not necessarily
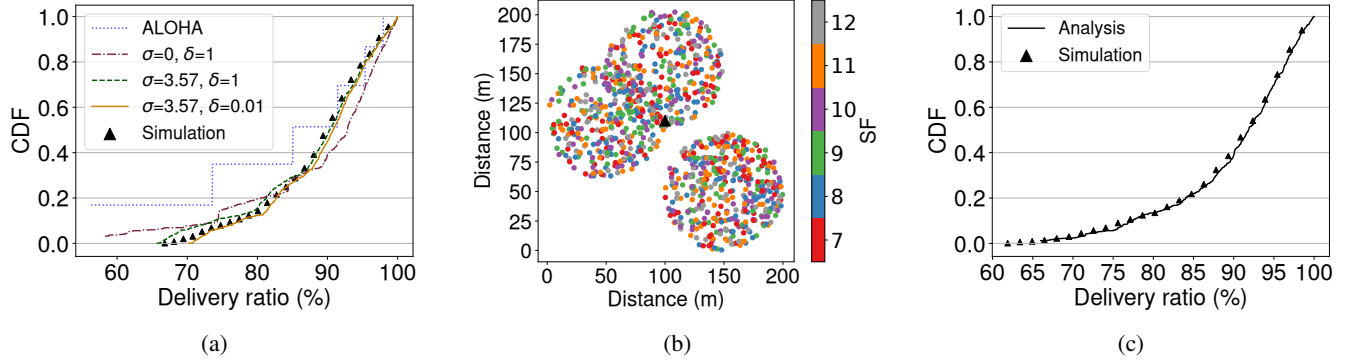
Fig. 6: (a) CDF of different model variants. (b) Network layout and (c) CDF of delivery ratio in a network with node diversity.
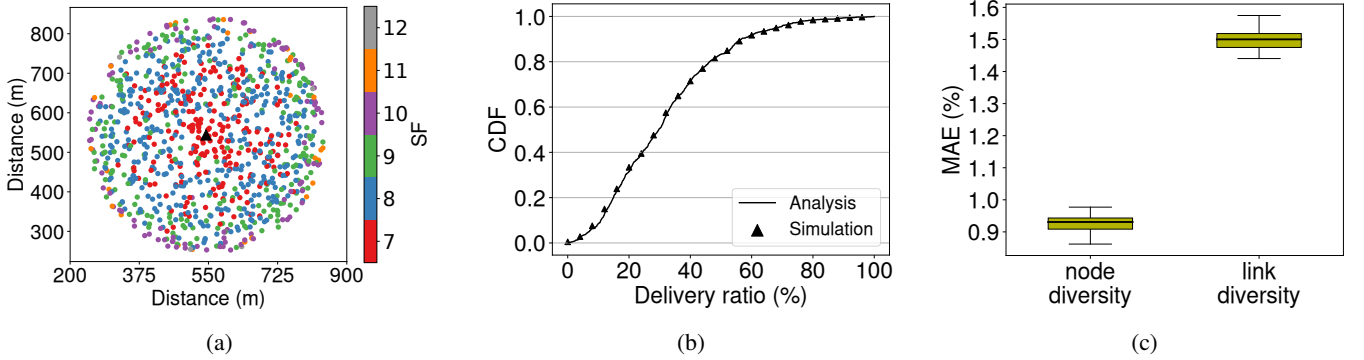

Fig. 7: (a) Network layout and (b) CDF of delivery ratio in an ADR-based network. (c) MAE for networks with node diversity and ADR-based configuration.

based on the distance of nodes from a gateway.

The following set of articles present analytical models for LoRa networks as extensions of the ALOHA model. Bankov et al. [21] model the delivery ratio in LoRa networks with a single gateway, taking into account the capture effect and re-transmissions. However, they do not include fading or inter-SF interference. Croce et al. [22] present a model for estimating the delivery ratio per spreading factor in a LoRa network with more than one gateway. In contrast to our solution, they do not include fading or duty cycle constraints and assume that all nodes use the same transmission power. Caillouet et al. [14] present a model for delivery ratio that takes into account the capture effect and interference between spreading factors. However, they do not include duty cycle constraints and all nodes are required to use the same transmission power. Furtado et al. [35] consider a model to estimate the delivery ratio in LoRa networks. Their model assumes that nodes are uniformly distributed around the gateway and that gateways can decode multiple frames transmitted with the same spreading factor (which is not currently supported by LoRa chipsets). As such, the focus of the article is only on evaluating networks with a single spreading factor and gateway. In contrast to the models presented above, the model in this article supports different network layouts (with one or more gateways) and does not restrict the assignment of spreading factors or transmission powers. Moreover, it incorporates the impact of duty cycle

restrictions and fading to support a more complete and realistic evaluation of LoRa networks.

V. CONCLUSION

This article presents an analytical model to accurately derive the delivery ratio of individual devices in realistic LoRa networks. Specifically, the model effectively characterizes the impact of quasi-orthogonal transmissions under the capture effect, duty cycling, multiple gateways, and shadow fading on network performance. Extensive simulations in networks with various layouts and link-level parameter settings show that the proposed model accurately estimates the delivery ratio of each device. Moreover, the proposed model provides a level of detail that is not available in the state of the art, and it matches the simulation results within an error of a few percentage points. Such an analytical model is valuable as it allows the flexible evaluation of different network scenarios, and provides insights into the optimal assignment of LoRa transmission parameters. A promising future work is to utilize the presented analytical model to derive optimal LoRa parameters such that *all* nodes communicate with high reliability.

References

[1] Semtech, "What is LoRa?" https://www.semtech.com/lora/what-is-lora, [Online; Accessed on 12.08.2020].

[2] J. P. S. Sundaram, W. Du, and Z. Zhao, "A survey on LoRa networking: Research problems, current solutions, and open issues," *IEEE Communications Surveys & Tutorials*, vol. 22, no. 1, pp. 371–388, 2019.

[3] LoRa Alliance, "LoRaWAN Specification (v1.0.3)," https://www.lora-alliance.org/resource-hub/lorawantm-specification-v103, Mar. 2018, [Online; Accessed on 11.08.2020].

[4] Semtech, "Real-world LoRaWAN Network Capacity for Electrical Metering Applications," https://cdn2.hubspot.net/hubfs/2507363/Semtech_Network_Capacity_White_Paper.pdf, [Online; Accessed on 15.08.2020].

[5] N. Varsier and J. Schwoerer, "Capacity limits of LoRaWAN technology for smart metering applications," in *2017 IEEE International Conference on Communications (ICC)*. IEEE, 2017, pp. 1–6.

[6] Z. Li, T.-B. Nguyen, Q. Lampin, I. Sivignon, and S. Zozor, "Ensuring k-coverage in low-power wide area networks for Internet of Things," in *2017 International Conference on Computing, Networking and Communications (ICNC)*. IEEE, 2017, pp. 26–30.

[7] M. C. Bor, U. Roedig, T. Voigt, and J. M. Alonso, "Do LoRa Low-Power Wide-Area Networks Scale?" in *Proceedings of the 19th ACM International Conference on Modeling, Analysis and Simulation of Wireless and Mobile Systems*, New York, NY, USA, 2016, p. 59:67.

[8] Semtech, "Smart parking - LoRa application brief," https://lora-developers.semtech.com/uploads/documents/files/Semtech_Cities_SmartParking_AppBrierf-FINAL.pdf, [Online; Accessed on 15.08.2020].

[9] A. Mahmood, E. Sisinni, L. Guntupalli, R. Rondón, S. A. Hassan, and M. Gidlund, "Scalability analysis of a LoRa network under imperfect orthogonality," *IEEE Transactions on Industrial Informatics*, vol. 15, no. 3, pp. 1425–1436, 2018.

[10] G. Premsankar, B. Ghaddar, M. Slabicki, M. Di Francesco *et al.*, "Optimal configuration of LoRa networks in smart cities," *IEEE Trans. Ind. Inform*, vol. 16, no. 12, pp. 7243–7254, 2020.

[11] Y. Li, J. Yang, and J. Wang, "DyLoRa: Towards Energy Efficient Dynamic LoRa Transmission Control," in *IEEE INFOCOM 2020-IEEE Conference on Computer Communications*. IEEE, 2020, pp. 2312–2320.

[12] J. Petajajarvi, K. Mikhaylov, A. Roivainen, T. Hanninen, and M. Pettissalo, "On the coverage of LPWANs: range evaluation and channel attenuation model for LoRa technology," in *2015 14th International Conference on ITS Telecommunications (ITST)*, 2015, pp. 55–59.

[13] N. Blenn and F. Kuipers, "LoRaWAN in the wild: Measurements from the things network," *arXiv preprint arXiv:1706.03086*, 2017.

[14] C. Caillouet, M. Heusse, and F. Rousseau, "Optimal SF allocation in LoRaWAN considering physical capture and imperfect orthogonality," in *2019 IEEE Global Communications Conference (GLOBECOM)*. IEEE, 2019, pp. 1–6.

[15] M. Slabicki, G. Premsankar, and M. Di Francesco, "Adaptive configuration of LoRa networks for dense IoT deployments," in *NOMS 2018 - 2018 IEEE/IFIP Network Operations and Management Symposium*, 2018, pp. 1–9.

[16] O. Georgiou and U. Raza, "Low power wide area network analysis: Can LoRa scale?" *IEEE Wireless Communications Letters*, vol. 6, no. 2, pp. 162–165, 2017.

[17] U. Raza, P. Kulkarni, and M. Sooriyabandara, "Low Power Wide Area Networks: An Overview," *IEEE Communications Surveys Tutorials*, vol. 19, no. 2, pp. 855–873, 2017.

[18] A. Waret, M. Kaneko, A. Guitton, and N. El Rachkidy, "LoRa throughput analysis with imperfect spreading factor orthogonality," *IEEE Wireless Communications Letters*, vol. 8, no. 2, pp. 408–411, 2018.

[19] A. Duda and M. Heusse, "Spatial issues in modeling LoRaWAN capacity," in *Proceedings of the 22nd International ACM Conference on Modeling, Analysis and Simulation of Wireless and Mobile Systems*, 2019, pp. 191–198.

[20] L. Beltramelli, A. Mahmood, M. Gidlund, P. Österberg, and U. Jennehag, "Interference modelling in a multi-cell LoRa system," in *2018 14th International Conference on Wireless and Mobile Computing, Networking and Communications (WiMob)*. IEEE, 2018, pp. 1–8.

[21] D. Bankov, E. Khorov, and A. Lyakhov, "Mathematical model of LoRaWAN channel access with capture effect," in *2017 IEEE 28th Annual International Symposium on Personal, Indoor, and Mobile Radio Communications (PIMRC)*. IEEE, 2017, pp. 1–5.

[22] D. Croce, M. Gucciardo, S. Mangione, G. Santaromita, and I. Tinnirello, "LoRa technology demystified: From link behavior to cell-level performance," *IEEE Transactions on Wireless Communications*, vol. 19, no. 2, pp. 822–834, 2019.

[23] T. Rappaport, *Wireless communications: principles and practice*. Prentice hall, 2002, vol. 2.

[24] J. Robert, S. Rauh, H. Lieske, and A. Heuberger, "IEEE 802.15 Low Power Wide Area Network (LPWAN) PHY Interference Model," in *2018 IEEE International Conference on Communications (ICC)*, 2018, pp. 1–6.

[25] F. Adelantado, X. Vilajosana, P. Tuset-Peiro, B. Martinez, J. Melia-Segui, and T. Watteyne, "Understanding the limits of LoRaWAN," *IEEE Communications Magazine*, vol. 55, no. 9, pp. 34–40, 2017.

[26] D. Croce, M. Gucciardo, S. Mangione, G. Santaromita, and I. Tinnirello, "Impact of LoRa imperfect orthogonality: Analysis of link-level performance," *IEEE Communications Letters*, vol. 22, no. 4, pp. 796–799, 2018.

[27] T. H. Nguyen, W. Jung, L. T. Tu, T. V. Chien, D. Yoo, and S. Ro, "Performance Analysis and Optimization of the Coverage Probability in Dual Hop LoRa Networks With Different Fading Channels," *IEEE Access*, vol. 8, pp. 107 087–107 102, 2020.

[28] G. Bianchi, F. Cuomo, D. Garlisi, and I. Tinnirello, "Sequential Waterfilling for Adaptive Data Rate allocation in LoRaWAN," *CoRR*, vol. abs/1907.12360, 2019. [Online]. Available: http://arxiv.org/abs/1907.12360

[29] M. Haenggi and R. K. Ganti, *Interference in Large Wireless Networks*. Foundation and trends in networking, 2009, vol. 3, no. 2.

[30] Z. Ajami and S. Cohen, "Enumerating minimal weight set covers," in *2019 IEEE 35th International Conference on Data Engineering (ICDE)*, April 2019, pp. 518–529.

[31] J. Beasley, "An algorithm for set covering problem," *European Journal of Operational Research*, vol. 31, no. 1, pp. 85 – 93, 1987.

[32] A. Caprara, P. Toth, and M. Fischetti, "Algorithms for the set covering problem," *Annals of Operations Research*, vol. 98, no. 1, pp. 353–371, Dec 2000.

[33] C. M. Grinstead and J. L. Snell, *Introduction to Probability*. American Mathematical Society, 2012.

[34] F. Cuomo, J. C. C. Gámez, A. Maurizio, L. Scipione, M. Campo, A. Caponi, G. Bianchi, G. Rossini, and P. Pisani, "Towards traffic-oriented spreading factor allocations in LoRaWAN systems," in *2018 17th Annual Mediterranean Ad Hoc Networking Workshop (Med-Hoc-Net)*. IEEE, 2018, pp. 1–8.

[35] A. Furtado, J. Pacheco, and R. Oliveira, "PHY/MAC uplink performance of Class A LoRa networks," *IEEE Internet of Things Journal*, vol. 7, no. 7, pp. 6528–6538, 2020.